

The fast spin-rotation of a young extra-solar planet

Ignas A. G. Snellen¹, Bernhard R. Brandl¹, Remco J. de Kok^{1,2}, Matteo Brogi¹, Jayne Birkby¹, and Henriette Schwarz¹

¹*Leiden Observatory, Leiden University, Postbus 9513, 2300 RA Leiden, The Netherlands*

²*SRON, Sorbonnelaan 2, 3584 CA Utrecht, The Netherlands*

The spin-rotation of a planet arises from the accretion of angular momentum during its formation^{1,2,3}, but the details of this process are still unclear. In the solar system, the equatorial rotation velocities and spin angular momentum of the planets show a clear trend with mass⁴, except for Mercury and Venus which have significantly spun down since their formation due to tidal interactions^{5,6}. Here we report on near-infrared spectroscopic observations at $\lambda/\Delta\lambda=100,000$ of the young extra-solar gas giant β Pictoris b^{7,8}. The absorption signal from carbon monoxide in the planet's thermal spectrum is found to be blueshifted with respect to the velocity of the parent star by (-15 ± 1.7) km sec⁻¹, consistent with a circular orbit⁹. The combined line profile exhibits a rotational broadening of 25 ± 3 km sec⁻¹, meaning that β Pictoris b spins significantly faster than any planet in the solar system, in line with the extrapolation of the known trend in spin velocity with planet mass.

Near-infrared high-dispersion spectroscopy has been used to characterize the atmospheres of hot Jupiters in close-in orbits¹⁰⁻¹¹. Such observations utilize changes in the radial component of the orbital velocity of the planet (resulting in changes in Doppler shift) to filter out the quasi-stationary telluric and stellar contributions in the spectra. Here we make use of the spatial separation and the difference in spectral signature between the planet and star, which allow the starlight to be filtered out. A similar technique¹² has been applied very successfully¹³ at a medium spectral dispersion to characterize the exoplanet HR8799c. We observed the β Pictoris system^{7,8} (K=3.5) using the Cryogenic high-Resolution InfraRed Echelle Spectrograph CRIRES¹⁴ located at the Nasmyth focus of UT1 of the Very Large Telescope (VLT) of the European Southern Observatory (ESO) at Cerro Paranal in Chile on the night of 17 December 2013, with the slit oriented in such way that it encompassed the planet and star.

An important step in the data analysis is the optimal removal of the stellar contribution along the slit, which for this A-star consists mostly of a telluric absorption spectrum. The resulting spectra were cross-correlated with theoretical spectral templates constructed in a similar way as in our previous work on hot Jupiters¹⁰⁻¹¹, varying the planet's atmospheric temperature pressure (T/p) profile, the carbon monoxide abundance and that of water vapor and methane, which can also show features in the

observed wavelength range. Note that there is a strong degeneracy between the atmospheric T/p profile and the abundance of the molecular species, meaning that different combinations of these parameters result in nearly identical template spectra.

At the expected planet position a broad and blue-shifted signal is apparent (see Figure 1), which is strongest when the cross-correlation is performed with a spectral template from an atmospheric model with deep carbon monoxide lines and a small contribution from water. We estimate the signal to have a SNR of 6.4 by cross-correlating the residual spectrum with a broadened model template, and compare the peak of the cross-correlation profile with the standard deviation. If we use the cross-correlation profile as seen in Figure 1 to estimate the SNR, we need to take into account the width of the signal and the dependence of adjacent pixels in the profile. This results in an SNR of 7.8, but this latter method we found to be less accurate, since it does not properly include contributions from correlated noise structures on scales of the broad signal. Cross-correlation with the optimal spectrum of water vapor alone provides a marginal signal at SNR~2, which means we cannot claim a firm detection of water in the planet atmosphere. No signal is retrieved for methane models (see Extended Data Fig. 1).

We fit the planet profile using a grid of artificial cross-correlation functions, produced by cross-correlating the optimal template spectrum with a broadened and velocity-shifted copy of itself, for a range of velocities and rotational broadening functions. The best fit (left panel of Figure 2) was obtained for a blue-shifted radial velocity of -15.4 ± 1.7 km sec⁻¹ (1σ , including the uncertainties in the system velocity, $+20 \pm 0.7$ km sec⁻¹, of the star¹⁵) and a rotational broadening of 25 ± 3 km sec⁻¹ (1σ), with the uncertainties estimated from chi-squared analysis. Cross-correlation with other less optimal model templates give only small variations in these values at the $< 0.3\sigma$ level (see Methods section). Monitoring the position of the planet over the last decade⁹ has resulted in an estimate of the orbital radius of 8 - 9 AU and an orbital period of 17-20 years. The planet ephemeris⁹, assuming a circular orbit, provides a planet radial velocity relative to the star of 13.2 - 14.1 km sec⁻¹ (1σ) either towards or away from us. This means there is no evidence for an eccentric orbit from our one planet radial velocity measurement. Since the orbital inclination has been constrained⁹ to $>86.8^\circ$, the planet has a ~20% probability to transit its parent star. Marginal evidence was presented for a possible transit event^{16,17} in 1981. That the planet is now moving towards us means that it is approaching inferior conjunction in the period 2017.5-2018.5, and previously during 1998-2001 and 1978-1984. This is consistent with a transit event in 1981. Note that if this event is spurious, there was an a priori probability of 50% for the direction (e.g. clockwise or anti-clockwise) of the planet motion to be consistent with the 1981 event.

The equatorial spin-rotation velocity of $V_{\text{spin}} = 25 \text{ km sec}^{-1}$ of β Pictoris b is higher than for any planet in the Solar-System. The Solar System planets show a clear correlation between their equatorial rotation velocity (or spin angular momentum) and mass⁴ (see the right panel of Figure 2), the former ranging from 0.24 km sec^{-1} for Mars to 13.3 km sec^{-1} for Jupiter. Both Mercury and Venus have dropped significantly below this relation since they have spun down from the tidal interactions with the Sun^{5,6}. Also the Earth has slowed down due to the gravitational interaction with the Moon¹⁸. The origin of the V_{spin} -mass relation is not known, but must be linked to the mass accretion processes during planet formation. The mass of β Pictoris b is highly uncertain, with estimates depending strongly on the time since its formation. A commonly used age estimate for the β Pictoris system is $(12^{+8}_{-4}) \text{ Myr}$, resulting in mass estimates^{19,20} of $(7^{+4}_{-3}) M_{\text{Jup}}$ to $(10^{+3}_{-2}) M_{\text{Jup}}$. However, recently, lithium depletion in the β Pictoris moving group²¹ suggests an age of $21 \pm 4 \text{ Myr}$, which would increase these planet mass estimates by $\sim 30\%$. We therefore adopt a planet mass of $11 \pm 5 M_{\text{Jup}}$. As can be seen in panel b of Figure 2, β Pictoris b appears broadly consistent with an extrapolation of the solar system V_{spin} -mass relation to higher planet masses. However, the spread in measured projected spin velocities of L4-L7 brown dwarfs^{22,23} (open circles) suggest a more complicated relationship for the general population of substellar objects. Furthermore, despite rotating faster than any planet in the solar system, β Pictoris b does appear to have a lower V_{spin} than expected from a direct extrapolation of the solar system trend, which would point to a spin velocity of $50 \pm 12 \text{ km sec}^{-1}$. This may well be because the planet is still young and warm ($1575\text{-}1650 \text{ K}$) and therefore bloated. Although the radius of the planet cannot be measured directly as in the case of transiting planets, spectral modeling¹⁹ of broadband photometry obtained by direct imaging provides an estimate of $1.65 \pm 0.06 R_{\text{Jup}}$. It implies a rotation period, the length of day on β Pictoris b, of $\sim 8.1 \pm 1.0 \text{ hours}$. Over the next hundreds of millions of years the planet is expected to cool down and shrink to the size of Jupiter²⁴. If its angular momentum is preserved during this process, the planet should spin up to $V_{\text{spin}} \sim 40 \text{ km sec}^{-1}$, depending on possible changes in its internal structure, decreasing its length of day to $\sim 3 \text{ hours}$. The reader should note that in the above we assume that the obliquity, the axial tilt of the planet, is small – which may not be the case, as we know from Uranus. However, even if we assume that the distribution of obliquities of extra-solar gas giants is random, the average component in the direction of Earth is 30° , resulting in an underestimate of V_{spin} of only $1 / \cos(30^\circ) = 15\%$.

Methods Summary

We targeted the 2-0 R-branch of carbon monoxide absorption using the two central detectors of CRIRES, resulting in a wavelength range of 2.303 to $2.331 \mu\text{m}$. The CRIRES slit (width= $0.2''$) was

oriented at 30° North through East to encompass the planet, which, according to recent high-contrast imaging observations, was located 0.4" South-West from the host star^{19,20}. We utilized the Multi-Application Curvature Adaptive Optics system (MACAO)²⁵ in 1-1.3" seeing conditions. This resulted in a reduction of the starlight at the planet position of a factor 8 to 30 (depending on the seeing). Therefore, a certain planet/star contrast can be reached 8-30 times faster compared to 'classical' high-dispersion spectroscopy of hot Jupiters, because the noise in the final planet spectrum originates from the star. After basic calibrations, we optimally extracted a 1D spectrum for each position along the slit, and subsequently removed the stellar contribution for each position. The resulting spectra were cross-correlated with planet model spectra (Extended Data Fig.1), which were produced in a similar way as for our previous work on hot Jupiters¹⁰⁻¹².

The SNR that can be achieved on a planet spectrum for this type of observation is a strong function of telescope diameter D. This opens the way of obtaining two-dimensional maps of the planet using Doppler imaging, a technique used to map spot distributions on fast-rotating active stars²⁶⁻²⁹. Very recently, a first Doppler image map was produced for the nearby brown dwarf Luhman 16B (K=9.73) using CRIRES on the VLT, showing large-scale bright and dark features, indicative of patchy clouds²³. The planet β Pictoris b is only a factor 13 fainter than Luhman 16B. Our simulations (Extended Data Fig.2) show that a similar study can be conducted on β Pictoris b using future instrumentation.

References

1. Lissauer, J. J., Kary, D. M., The origin of the systematic component of planetary rotation. I - Planet on a circular orbit, *Icarus* **94**, 126-159 (1991)
2. Dones, L., Tremaine, S., On the origin of planetary spins, *Icarus* **103**, 67-92 (1993)
3. Johansen, A., Lacerda, P., Prograde rotation of protoplanets by accretion of pebbles in a gaseous environment, *Mon. Not. R. Astron. Soc.* **404**, 475-485 (2010)
4. Hughes, D. W., Planetary spin, *Planetary and Space Science* **51**, 517-523 (2003)
5. Pettengill, G. H., Dyce, R. B., A Radar Determination of the Rotation of the Planet Mercury, *Nature* **206**, 1240 (1965)
6. Correia, A. C. M., Laskar, J., The four final rotation states of Venus, *Nature* **411**, 767-770. (2001)
7. Lagrange, A.- M., Gratadour, D., Chauvin, G.; Fusco, T., Ehrenreich, D., Mouillet, D., Rousset, G., Rouan, D., Allard, F., Gendron, É., Charton, J., Mugnier, L., Rabou, P., Montri, J., Lacombe, F., A probable giant planet imaged in the β Pictoris disk, *Astron. Astrophys.* **493**, L21-L25 (2009)
8. Lagrange, A.- M., Bonnefoy, M., Chauvin, G., Apai, D., Ehrenreich, D., Boccaletti, A., Gratadour,

- D., Rouan, D., Mouillet, D., Lacour, S., Kasper, M., A Giant Planet Imaged in the Disk of the Young Star Pictoris, *Science* **329**, 57–59 (2010)
9. Chauvin, G., Lagrange, A.-M., Beust, H., Bonnefoy, M., Boccaletti, A., Apai, D., Allard, F., Ehrenreich, D., Girard, J. H. V., Mouillet, D., Rouan, D., Orbital characterization of the β Pictoris b giant planet, *Astron. Astrophys.* **542**, A41 (2012)
10. Brogi, M., Snellen, I., de Kok, R., Albrecht, S., Birkby, J., de Mooij, E., The signature of orbital motion from the dayside of the planet tau Bootis b, *Nature* **486**, 502-504 (2012)
11. de Kok, R., Brogi, M., Snellen, I., Birkby, J., Albrecht, S., de Mooij, E., Detection of carbon monoxide in the high-resolution day-side spectrum of the exoplanet HD 189733b, *Astron. Astrophys.* **554**, A82 (2013)
12. Sparks, W.B. & Ford, H.C., Imaging Spectroscopy for Extrasolar Planet Detection, *Astrophys. J.* **578**, 543 (2002)
13. Konopacky, Q.M., Barman, T.S., Macintosh, B.A., Marois, C., Detection of Carbon Monoxide and Water Absorption Lines in an Exoplanet Atmosphere, *Science* **339**, 1398-1401 (2013)
14. Kaeufl, H.-U., et al., CRIRES: a high-resolution infrared spectrograph for ESO's VLT., Ground-based Instrumentation for Astronomy 5492, 1218-1227 (2004)
15. Gontcharov, G. A., Pulkovo Compilation of Radial Velocities for 35495 Hipparcos stars in a common system, *Astronomy Letters* **32**, 759-771 (2006)
16. Lecavelier Des Etangs, A., Deleuil, M., Vidal-Madjar, A., Ferlet, R., Nitschelm, C., Nicolet, B., Lagrange-Henri, A. M., beta Pictoris: evidence of light variations, *Astron. Astrophys.* **299**, 557 (1995)
17. Lecavelier Des Etangs, A., Vidal-Madjar, A., Burki, G., Lamers, H., Ferlet, R., Nitschelm, C., Sevre, Beta Pictoris light variations. I. The planetary hypothesis, *Astron. Astrophys.* **328**, 311-320 (1997)
18. Cuk, M., Stewart, S., Making the Moon from a Fast-Spinning Earth: A Giant Impact Followed by Resonant Despinning, *Science* **338**, 1047 (2012)
19. Currie, T., Burrows, A., Madhusudhan, N., Fukagawa, M., Girard, J., Dawson, R., Murray-Clay, R., Kenyon, S., Kuchner, M., Matsumura, S., Jayawardhana, R., Chambers, J., Bromley, B., A Combined Very Large Telescope and Gemini Study of the Atmosphere of the Directly Imaged Planet, β Pictoris b, *Astrophys. J.* **776**, 15 (2013)
20. Bonnefoy, M., et al, The near-infrared spectral energy distribution of beta Pictoris b, *Astron. Astrophys.* **555**, A107 (2013)
21. Binks A.S, Jeffries R.D., A lithium depletion boundary age of 21 Myr for the Beta Pictoris moving group, *Mon. Not. R. Astron. Soc.* **438**, L11-L15 (2014)
22. Konopacky Q.M., Ghez A.M., Fabrycky D.C., Macintosh B.A., White R.J., et al., Rotational

- velocities of individual components in very low mass binaries, *Astroph. J.* **750**, 79-93 (2012)
23. Crossfield, I., et al., A Global Cloud Map of the Nearest Known Brown Dwarf, *Nature* **505**, 654–656 (2014)
24. Baraffe I., Chabrier G., Barman T.S., Allard F., Hauschildt P.H., Evolutionary models for cool brown dwarfs and extrasolar giant planets, *Astron. Astrophys.* **402**, 701-712 (2003)
25. Arsenault, R., et al., MACAO-VLTI: An Adaptive Optics system for the ESO VLT interferometer, *Adaptive Optical System Technologies II* **4839**, 174-185. (2003)
26. Vogt, S., Penrod, G., Doppler Imaging of spotted stars - Application to the RS Canum Venaticorum star HR 1099, *Publications of the Astronomical Society of the Pacific* **95**, 565-576 (1983)
27. Vogt, S., Hatzes, A., Misch, A., Kurster, M., Doppler Imagery of the Spotted RS Canum Venaticorum Star HR 1099 (V711 Tauri) from 1981 to 1992, *Astrophys. J. Suppl.* **121**, 547-589 (1999)
28. Barnes, J., Collier Cameron, A., James, D., Donati, J.-F., Doppler images from dual-site observations of southern rapidly rotating stars - I. Differential rotation on PZ Tel, *Mon. Not. R. Astron. Soc.* **314**, 162-174 (2000)
29. Vogt, S., Penrod, G., Hatzes, A., Doppler images of rotating stars using maximum entropy image reconstruction. *Astrophys. J.* **321**, 496-515 (1987)

Acknowledgements We thank ESO director Tim de Zeeuw for granting Director's Discretionary Time on the Very Large Telescope to perform these observations (292.C-5017(A)). I.S. acknowledges support from an NWO VICI grant. R.d.K acknowledges the NWO PEPSci program.

Author Contributions I.S. conceived the project with help from B.B, R.d.K, M.B, J.B. The analysis was led by I.S. and he wrote the first version of the manuscript. I.S. and B.B. conceived the connection with the ELT. R.d.K constructed the planet atmosphere models. B.B, R.d.K, M.B., J.B., and H.S. discussed the analyses, results, and commented on the manuscript.

Author Information The authors declare no competing financial interests. Correspondence and request for materials should be addressed to I.S. (e-mail: snellen@strw.leidenuniv.nl).

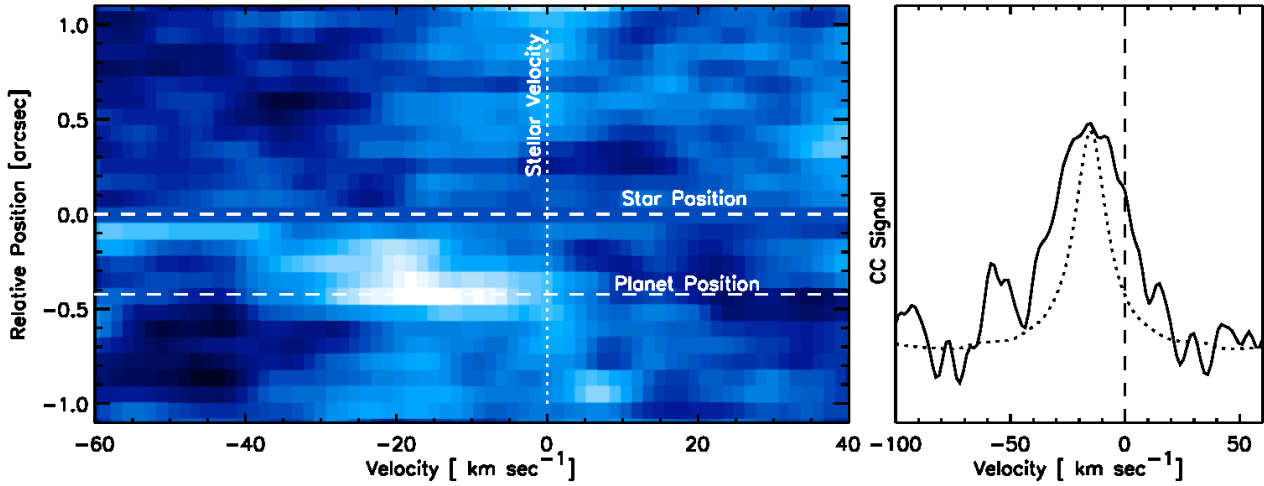


Figure 1. The broadened cross-correlation signal of β Pictoris b. Panel a) shows the CO+H₂O cross-correlation (CC) signal as function of the position along the slit (rotated by 30° North to East), after the stellar contribution was removed. The x-axis shows the radial velocity with respect the system velocity ($+20 \pm 0.7 \text{ km sec}^{-1}$) of the star¹⁵. The y-axis denotes the relative position with respect to the star β Pictoris with the planet located 0.4'' below, both indicated by horizontal dashed lines. A broad signal, at an SNR of 6.4 is visible, blue-shifted by $-15.4 \pm 1.7 \text{ km sec}^{-1}$ (1σ) with respect to the system velocity. Panel b) shows the CC signal at the planet position. The dotted curve shows the arbitrarily scaled auto-correlation function of the $\lambda/\Delta\lambda=100,000$ model template, indicating the CC-signal expected from a non-rotating planet.

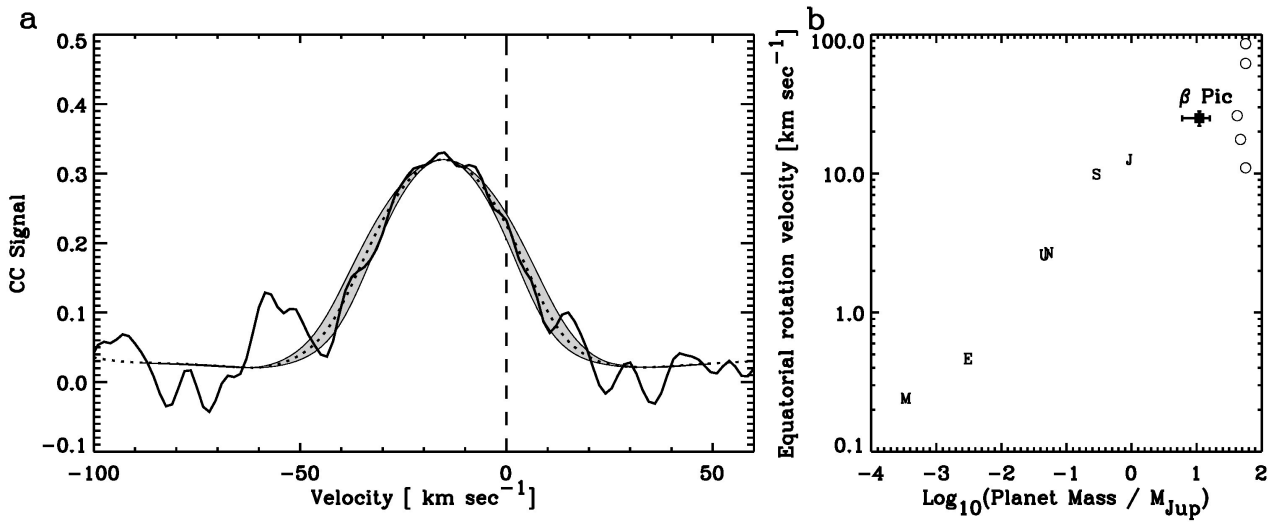


Figure 2. The Spin-rotation of β Pictoris b. Panel a) shows the CO+H₂O cross correlation signal of the planet β Pictoris b (solid line). The dashed line indicates the best fit to the cross-correlation profile of the model template with a copy of itself, rotationally broadened by 25 km sec⁻¹. The grey area indicates the 1 σ uncertainty in the level of broadening of ± 3 km sec⁻¹. Panel b) shows the equatorial rotation velocity of the solar system planets as function of planet mass, each planet indicated by its first letter. Note that Mercury and Venus are not visible on this plot. Tidal interactions with the Sun made these planets to significantly spin down to $V_{\text{spin}} \ll 0.1$ km sec⁻¹. β Pictoris b is indicated with a planet mass of $11^{+5} M_{\text{Jup}}$, consistent with the solar system mass- V_{spin} trend extended to higher masses. The open circles indicate the projected spin velocities of L4-L7 type brown dwarfs from refs 22 and 23.

Methods

Observations and Data Analysis

We targeted the 2-0 R-branch of carbon monoxide absorption using the two central detectors of CRIRES, resulting in a wavelength range of 2.303 to 2.331 μm . The slit (width=0.2") was oriented at 30° North through East to encompass the planet, which, according to recent high-contrast imaging observations, was located 0.4" South-West from the host star^{19,20}. We took 44 exposures of 4x10 seconds utilizing an ABBA dither pattern to enable accurate background subtraction. In addition, each dither position was given a small but random offset to minimize potential flat-fielding issues. We utilized the Multi-Application Curvature Adaptive Optics system (MACAO)²⁵ in 1-1.3" seeing conditions. This resulted in a reduction of the starlight at the planet position of a factor 8 to 30 (depending on the seeing). Therefore, a certain planet/star contrast can be reached 8-30 times faster compared to 'classical' high-dispersion spectroscopy of hot Jupiters, because the noise in the final planet spectrum originates from the star.

We performed the basic calibrations on the individual frames using the standard CRIRES reduction pipeline³⁰, including dark subtraction, flat fielding, and non-linearity corrections, after which the frames in the AB or BA pairs of two points along the slit were subtracted from each other. Subsequently, the frames of each pair of two-dimensional spectra were combined. The subsequent analysis was performed on the resulting 22 intermediate data products from the pipeline using IDL routines. We determined the spatial profiles of the star as function of wavelength, which we subsequently used to optimally extract a 1D spectrum for each position along the slit, in steps of one spatial pixel of 0.086", with the planet expected to be located about five pixels from the center of the star⁹. The combined spectrum of 30 pixel rows along the slit was taken as a reference of the stellar spectrum and used to remove the stellar contribution from each spatial pixel position along the slit – a crucial step in the data analysis. At the central position of the star, its spatial profile is narrow compared to the slit-width, resulting in a higher spectral resolution compared to elsewhere along the slit, in addition to a small wavelength offset because the star was not exactly centered in the slit. To remove the star light properly at each position along the slit, the reference spectrum not only had to be scaled, but also shifted and convolved with a broadening function. This broadening function was determined for each individual slit position and frame, using the Singular Value Decomposition technique³¹. The reader should note that the average reference spectrum contains planet light at a level of 1/8 to 1/30 of that at the planet position, marginally weakening the expected signal by that amount. The residual spectra as function of position along the slit for the 22 frames were subsequently combined, weighing the frames according to their varying (seeing induced) stellar profile, and thus maximizing the expected SNR of the final planet spectrum.

Planet model spectra were produced in a similar way as for our previous work on hot Jupiters^{10,11,32,33}. A uniform temperature-Pressure (T/p) profile was assumed to describe the vertical structure of the planet atmosphere, parameterized by two points, (T₁,p₁) and (T₂,p₂). Below and above these levels in the atmosphere the temperature was assumed to be constant at T₁ and T₂, respectively. At pressures p₁>p>p₂ a constant lapse rate was assumed as $\delta T/\delta \log_{10} p = (T_2 - T_1)/(\log_{10} p_2 - \log_{10} p_1)$. The model spectra were subsequently produced using line-by-line calculations including H₂-H₂ collision-induced absorption^{34,35} and absorption from three trace gases, i.e. CO, H₂O, and CH₄, which are the dominant sources of opacities at these wavelengths^{36,37}. Line data for the trace gases were taken^{38,39} from HITEMP 2010 for H₂O and CO, and HITRAN 2008 for CH₄. A Voigt line profile was used for the calculations.

Since large degeneracies exist between different models, we did not explore a full grid of models varying (T₁,p₁), (T₂,p₂) and the molecular abundances. This can be seen in Extended Data Figure 1, which shows the results of five different models, with the parameters indicated in the title. The two top models have a CO volume mixing ratio (VMR) that differ by three orders of magnitude (VMR_{CO}=10^{-1.5} versus 10^{-4.5}), but both show a strong signal. If we mix in other molecules, the significance of the detected signal becomes lower. This can be seen by cross-correlating with the third model, which is for a low CO and high H₂O VMR, showing that the signal is still visible but at a significantly lower SNR than above. This is in line with the fourth model spectrum consisting of H₂O only, which gives only a marginal detection at SNR~2. We therefore cannot claim a firm detection of water vapour in this planet atmosphere. The last model is for CH₄ only – showing no signal.

Doppler Imaging simulations

High-dispersion spectral observations that aim to characterize exoplanet atmospheres have so far been restricted to hot Jupiters in very close-in orbits. Such observations utilize changes in the radial component of the orbital velocity of the planet (resulting in changes in Doppler shift) to filter out the quasi-static telluric and stellar contributions in the spectra. Here we use high-dispersion spectroscopy to characterize the young gas giant β Pictoris b, which was previously discovered using high-contrast imaging techniques. These observations make use of the angular separation and the spectral differences between the planet and the star. While the planet to star contrast is about 3800 at 2.3 μ m, the starlight is reduced by a factor 8 to 30 (varying with the seeing) at the planet position 0.4" away, making the planet-light buried at a level 1/500th to 1/100th in the wing of the stellar spatial profile. This stellar contribution, which is dominated by telluric absorption, can be filtered out very effectively since this spectrum is well determined along the slit, albeit with small variations in the spectral dispersion which are taken into account, and it is therefore known at a very high signal to noise. A

similar technique¹² has been applied very successfully¹³ at a medium spectral dispersion to characterize the exoplanet HR8799c.

The relative ease at which the presented detection was obtained is noteworthy, using only 1 hour of observing time (including overheads) on an 8m-class telescope in mediocre seeing. If the CO signal was not smeared out over -25 to $+25$ km sec⁻¹ due to the planet rotation, but concentrated in an unresolved signal, it would have been detected at a SNR \sim 15. We also investigated the scientific potential of the future European Extremely Large Telescopes (E-ELT) for these kinds of observations. METIS, the Mid-infrared E-ELT Imager and Spectrograph⁴⁰, will have a $\lambda/\Delta\lambda=100,000$ integral field spectrograph in the 3-5 μ m wavelength range. This does not cover the 2.3 μ m CO, but H₂O at 3.2 or 3.5 μ m can also be targeted highly effectively. The absorption features are probably somewhat weaker than those of CO at 2.3 μ m, but both the planet/star contrast and the flux from the planet are more than a factor two higher. Alternatively, the HIRES spectrograph⁴¹ is expected to cover the optical to near-infrared wavelength regime, and can be used for this type of observation, if it is designed with a slit or with multiple fibers that can cover both the star and the planet. The other Extremely Large Telescope projects, the Giant Magellan Telescope⁴² and the Thirty Meter Telescope⁴³, also have optical and infrared high-resolution spectrographs in their instrument roadmaps.

In this work we focus on the E-ELT. For simplicity, we will assume a spectrograph concept similar to CRILES, using an adaptive optics system that produces similar Strehl ratios under the same atmospheric conditions. Since the angular resolution of the telescope scales with λ/D , with D the telescope diameter ($D=39$ m for the E-ELT), the angular distance of the planet from the star in units of diffraction elements will be a factor 4.8 larger. In our CRILES frames the starlight is suppressed by a factor \sim 500 at that distance. In addition, the apparent size of the planet is decreased by a factor D^2 , gaining another factor 23. This means that for similar observations with the E-ELT the starlight at the planet position will be reduced by a factor \sim 10⁴, meaning it only marginally contributes to the noise in the planet spectrum. It implies that with the E-ELT we will be able to observe the $K=12.5$ planet as if there were no nearby host star. We use the CRILES exposure time calculator, multiplying the number of observations by a factor 23 to account for the increase in collecting area, to estimate that an exposure of 100 seconds will deliver a $\lambda/\delta\lambda=100,000$ spectrum of the planet β Pictoris b with an SNR of \sim 25 per 1.5 km sec⁻¹ resolution element.

We subsequently take this value to simulate what we can learn about the atmosphere of β Pictoris b with the E-ELT using Doppler imaging techniques. Doppler imaging²⁶⁻²⁸ can map inhomogeneities on a rotator's surface by monitoring the distortions in rotationally broadened absorption lines. By

monitoring features in the velocity broadening function to appear, shift in velocity and disappear, the planet brightness distribution can be solved for using maximum entropy mapping²⁹, as done for stars. The reader should note that very recently, a first Doppler image map was produced for the nearby brown dwarf Luhman 16B (K=9.73) using CRIRES on the VLT, showing large-scale bright and dark features, indicative of patchy clouds²³. The planet β Pictoris b is a factor 13 fainter than Luhman 16B, meaning that such result can be obtained almost two times faster with the E-ELT for the planet, than with the VLT for the brown dwarf. To simulate this we have constructed a toy model map of the planet's atmospheric surface of 360x180 pixels with an uniform surface brightness, except for one spot twice as bright, at a latitude of +55° and with a radius of 10°. Note that we gave the planet an obliquity of 30°. A low spin-axial tilt will result in a degeneracy for features on opposite hemispheres, although this is not relevant for these forward simulations. We subsequently calculated the overall spectrum of the planet for three viewing angles, which are consecutively observed at one hour intervals. The CO model that fits our CRIRES data best is assigned to each pixel in the planet surface map. Subsequently, each surface-pixel visible from the modelled viewing angle attributed to the overall spectrum, Doppler shifted according to the radial component of its rotation velocity and weighed by the cosine of the local surface viewing-angle.

The three observations were simulated with an exposure time of 15 minutes each, meaning they have a SNR of 75 per resolution element. Gaussian noise was added to the three spectra accordingly. The three spectra were subsequently cross-correlated with the model spectrum, of which the result is shown in the right panel of Extended Data Figure 2. It shows the great potential of obtaining a 2D map of the planet by using maximum entropy mapping. This can lead to unique exploration tools, such as the monitoring of multiple spots or other atmospheric features like dark or bright bands at different planet latitudes, which can solve for effects from the planet obliquity, oblateness, limb darkening, and/or differential rotation.

30. CRIRES Data reduction pipeline:

http://www.eso.org/observing/dfo/quality/CRIRES/pipeline/pipe_gen.html

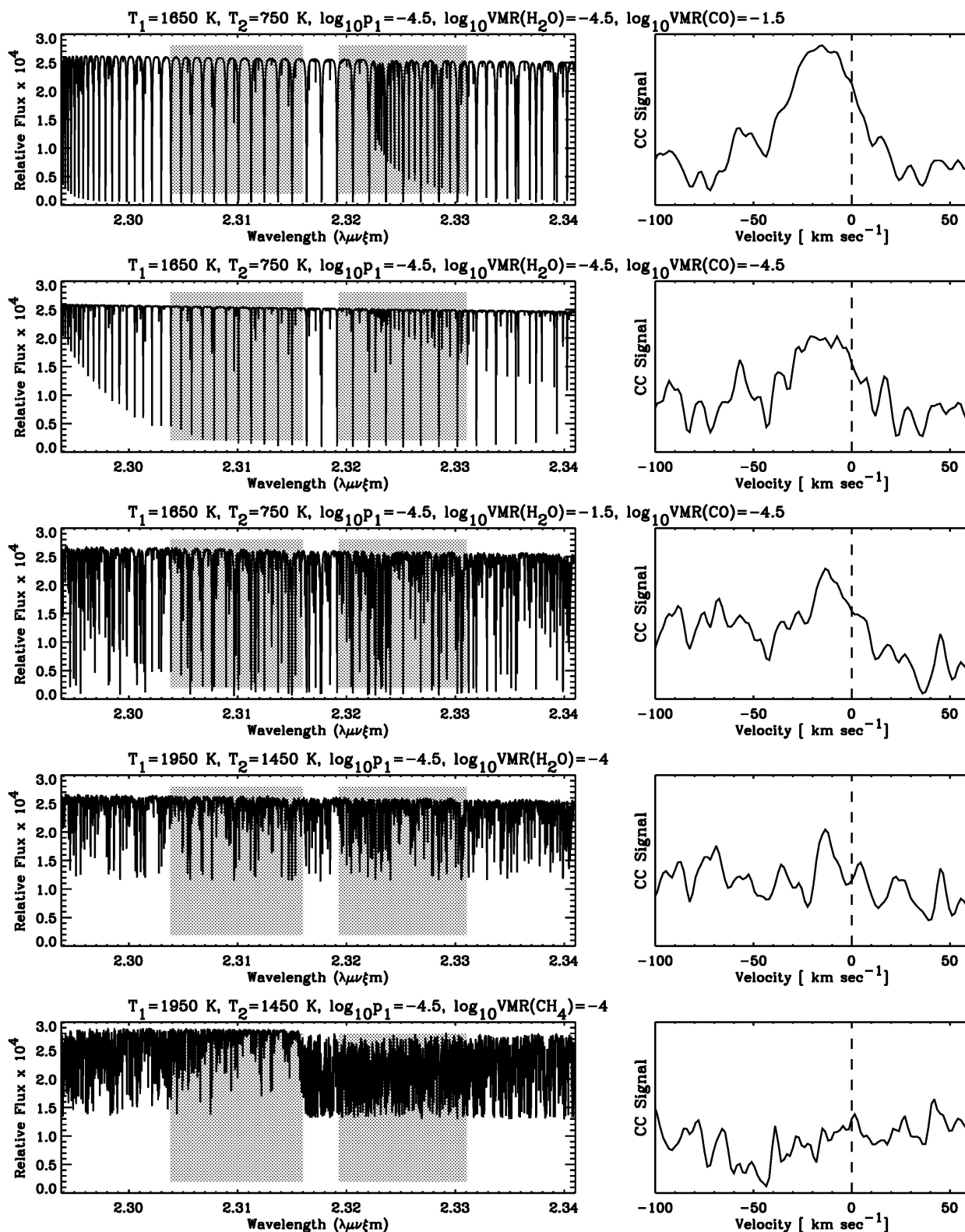
31. Rucinski, S., Determination of Broadening Functions Using the Singular-Value

Decomposition (SVD) Technique, *IAU Colloq. 170: Precise Stellar Radial Velocities* **185**, 82 (1999)

32. Brogi, M., Snellen, I., de Kok, R., Albrecht, S., Birkby, J., de Mooij, E. Detection of Molecular Absorption in the Dayside of Exoplanet 51 Pegasi b?, *Astrophys. J.* **767**, 27. (2013)

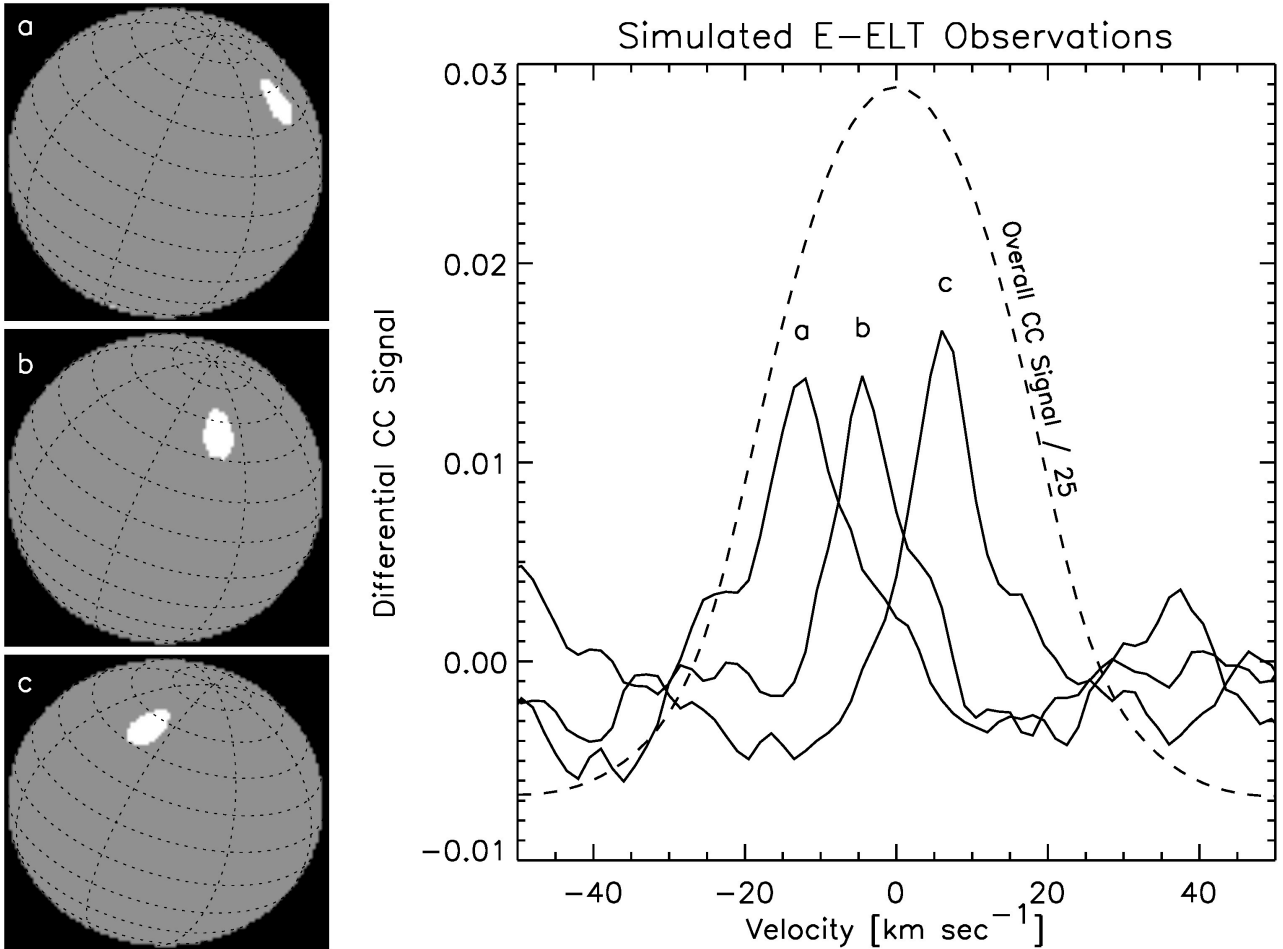
33. Birkby, J.L., de Kok, R.J., Brogi, M., de Mooij, E.J.W., Schwarz, H., Albrecht, S., Snellen, I.A.G.,

- Detection of water absorption in the day side atmosphere of HD 189733 b using ground-based high-resolution spectroscopy at 3.2 μm , *Mon. Not. R. Astron. Soc.* **436**, L35-L39 (2013)
34. Borysow, A. , Jorgensen U.G., Fu, Y, High-temperature (1000–7000 K) collision-induced absorption of H₂ pairs computed from the first principles, with application to cool and dense stellar atmospheres, *J. Quant. Spec. Radiat. Transf.* **68**, 235 (2001)
35. Borysow, A. 2002, Collision-Induced absorption coefficients of H₂ pairs at temperatures from 60 K to 1000 K, *Astron. Astroph.* **390**, 779 (2002)
36. Madhusudhan, N. 2012, C/O Ratio as a Dimension for Characterizing Exoplanetary Atmospheres, *Astrophys. J.* **758**, 36 (2012)
37. Moses, J. I., Madhusudhan, N., Visscher, C., & Freedman, R. S., Chemical Consequences of the C/O Ratio on Hot Jupiters: Examples from WASP-12b, CoRoT-2b, XO-1b, and HD 189733b, *Astrophys. J.* **763**, 25 (2013)
38. Rothman, L. S., Gordon, I. E., Barber, R. J., et al., HITEMP, the high-temperature spectroscopic database, *J. Quant. Spec. Radiat. Transf.* **111**, 2139 (2010)
39. Rothman, L. S., Gordon, I. E., Barbe, A., et al., The HITRAN 2008 molecular spectroscopic database, *J. Quant. Spec. Radiat. Transf.*, **110**, 533 (2009)
40. Brandl, B. et al., METIS: the thermal infrared instrument for the E-ELT, *Society of Photo-Optical Instrumentation Engineers (SPIE) Conference Series* **8446** (2012)
41. Maiolino R., et al., A Community Science Case for E-ELT HIRES, <http://arxiv.org/abs/1310.3163> (2013)
42. Lee, S., et al. GMTNIRS (Giant Magellan Telescope near-infrared spectrograph): design concept, *SPIE* **7735**, 87
43. <http://www.tmt.org/>



EXTENDED DATA FIGURE 1

Model Spectra and cross-correlation signals. The model spectral templates (left panels) and the resulting cross-correlation signals (right panels) for (from top to bottom), 1) a high VMR CO model, 2) a low VMR CO model, 3) the same but adding a high VMR of H_2O , 4) a H_2O only mode, and 5) a CH_4 model. Atmospheric pressures are in units of bar.



EXTENDED DATA FIGURE 2

Simulated E-ELT observations. We simulated observations using the future 39 m European Extremely Large Telescope (E-ELT) of a rotating spot on β Pictoris b. Such observations could be conducted with the planned METIS⁴⁰. The three panels on the left, denoted a, b, and c, show the position of the spot approximately 1 hour apart, which was given a surface brightness of twice of the rest of the planet atmosphere. The right panel shows the difference between three cross-correlation signals with respect to the average cross-correlation profile as indicated by the dashed curve (scaled down by a factor 25), with the spot signature moving from -15 to +5 km sec⁻¹.